Förster Resonance Energy Transfer Measurements Are Consistent with a Helical Bundle Model for Lipid-Free Apolipoprotein A-I†

Christie G. Brouillette,*,‡,§,|| Wen-Ji Dong,|| Zhengrong W. Yang,‡ Marjorie J. Ray,‡ Irina I. Protasevich,‡ Herbert C. Cheung,*,|| and Jeffrey A. Engler||

Center for Biophysical Sciences and Engineering, Department of Vision Sciences, and Department of Biochemistry and Molecular Genetics, University of Alabama at Birmingham, Birmingham, Alabama 35294

Received May 30, 2005; Revised Manuscript Received October 14, 2005

ABSTRACT: Apolipoprotein (apo) A-I mutants were constructed for FRET studies to distinguish between two possible lipid-free conformers, a globular helix bundle and an elongated helical hairpin. Mutants containing a single Trp at position 50 were prepared by replacing Trps at positions 8, 72, and 108 with Phe (W@50). Two mutants were constructed from W@50 by incorporating Cys at Arg83 (W@50R83C) or Arg173 (W@50R173C) for attachment of the fluorescent probe AEDANS. Secondary structure of the mutants is very similar to wild type (wt) apo A-I, and fluorescence emission indicates that W50 is protected from solvent. Thermal stabilities of the AEDANS-labeled mutants are also similar to wt. These results indicate that no discernible changes occur in structure or stability as a result of mutations or labeling. The FRET data from W@50 to AEDANS are well-represented by a single distance distribution function with a distance of ∼22 Å for W@50R83C and ∼19 Å for W@50R173C. These distances are consistent with theoretical values calculated from a helical bundle model but not from a helical hairpin. A probability distance distribution function yields significantly small half-width values of 5.6 and 3.7 Å, respectively, suggesting low conformational dynamics in both mutants. Differential scanning calorimetry (DSC) was performed on wt and a C-terminal deletion mutant, Δ(187−243), to obtain information on domain architecture. Contrary to expectations, both proteins unfold cooperatively. The results are consistent with the presence of a single folded domain within residues 1−186. These results support the presence of a discrete globular bundle conformation for lipid-free apo A-I.

Human apolipoprotein (apo) A-I is a 243-residue polypeptide containing a series of highly homologous 11- and 22-residue amphipathic α-helices. Apo A-I resides on the surface of high-density lipoprotein (HDL).[1] It comprises about 70% of total HDL protein and is generally viewed to be responsible for most functions of HDL. The breadth of functions attributed to apo A-I include lipid and cholesterol binding or solubilization, lecithin-cholesterol acyl transferase (LCAT) activation, antiinflammation, antioxidation, and binding to the ATP binding cassette A1 (ABCA1) transporter receptor.

The multiplicity of functions attributed to apo A-I suggests a need for a flexible and adaptable structure. The functions of apo A-I and HDL-bound apo A-I may therefore arise, in part, from its existing structural form and, in fact, a variety of data indicate that apo A-I adopts multiple, physiologically relevant, conformations (*1*−*5*). In addition to its lipid-bound form, as associated with discoidal and spherical HDL, apo A-I exists in plasma in various partially lipidated states, including so-called "lipid-poor" apo A-I and lipid-free apo A-I (found to be up to 5−10% of circulating apo A-I (*6*, *7*)). These forms are apparently in dynamic exchange as a result of metabolic enzymes that act upon HDL.

The presence of lipid-free and lipid-poor apo A-I in the plasma is likely of physiological importance to many, if not all, of its functions. Therefore, it is of interest to learn the structures of, and the mechanism for interconversion between, these functionally relevant conformations. With this in mind, a number of studies in the past decade have focused on the conformation of the lipid-free state of apo A-I (*8*−*21*). From these, an image of the protein's shape emerges that is not as much globular as it is elongated, or possibly even fluctuating between a globule and a more elongated form. The studies to date, therefore, leave open the question of which form dominates in solution.

† This work was supported, in part, by National Institutes of Health Grant R01HL61466 and Core Support from P30 CA-13148-34.

* To whom correspondence should be addressed: Christie G. Brouillette, UAB Center for Biophysical Sciences and Engineering, 1025 18th Street South, Birmingham, AL 35294. Tel: 205-975-5469; fax: 205-934-3352; e-mail: christie@uab.edu; Herbert C. Cheung, UAB Department of Biochemistry and Molecular Genetics, MCLM490, 1918 University Blvd., Birmingham, AL 35294. Tel: 205-934-2485; e-mail: ccheung@uab.edu.

‡ Center for Biophysical Sciences and Engineering.

§ Department of Vision Sciences.

|| Department of Biochemistry and Molecular Genetics.

[1] Abbreviations: AEDANS, 5-((((2-iodoacetyl)amino)ethyl)amino) naphthalene-1-sulfonic acid; apo, apolipoprotein; CD, circular dichroism; Da, dalton; EDTA, ethylenediamine tetraacetic acid; FRET, Förster resonance energy transfer; HDL, high-density lipoprotein; HEPES, 4-(2-hydroxyethyl)-1-piperazine ethane sulfonic acid; λ_{max}, maximum wavelength; LC MS, liquid chromatography mass spectrometry; RP HPLC, reversed phase high performance liquid chromatography; LCAT, lecithin-cholesterol acyl transferase; SDS−PAGE, sodium dodecyl sulfate−polyacrylamide gel electrophoresis; TCEP, tris(2-chloroethyl)-phosphate; TFA, trifluoroacetic acid; TOF MS, time-of-flight mass spectrometry; TRIS, tris(hydroxymethyl)aminomethane; UV, ultraviolet; wt, wild type.

10.1021/bi051018v CCC: $30.25
Published on Web 11/19/2005

Here, mutants were constructed that contain a single native tryptophan at position 50, W@50, by replacing native tryptophans with phenylalanine at positions 8, 72, and 108. Previously, all possible single tryptophan mutants of apo A-I (including one similar to W@50) were constructed by Davidson et al. for intrinsic fluorescence studies (not FRET) (*14*). In the present studies, a cysteine was also incorporated for attachment of the extrinsic fluorescent probe AEDANS. The amino acid position for cysteine replacement was selected so that energy transfer from W@50 in a helical bundle conformation would yield a distance easily distinguished from the distance measured if the protein was folded as an elongated hairpin. Two such mutants were constructed that met this criterion by replacing either arginine 83, or arginine 173, within the W@50 mutant: W@50R83C and W@50R173C. To aid in the interpretation of the FRET results, we built structural models for a globular helical bundle and an elongated hairpin of lipid-free apo A-I that are consistent with known structural data and derived from the intermolecular helix−helix interactions found in our crystal structure of apo Δ(1−43)A-I (*10*, *12*, *13*). The structural models and the FRET measurements are discussed in light of results from differential scanning calorimetry (DSC) that support a cooperative folded structure for apo A-I.

EXPERIMENTAL PROCEDURES

Construction and Expression of apo hA-I Cysteine Mutants. A pGEMEX (Promega, Madison, WI) plasmid containing a modified wt human apo hA-I gene with an N-terminal six-amino acid histidine tag and a four-amino acid Factor Xa cleavage site immediately prior to the start of the mature apo hA-I sequence was prepared as described elsewhere (*13*). Mutants were prepared using the QuickChange kit (Stratagene) with the modified apo hA-I plasmid as a template and pairs of complementary oligonucleotide primers designed to change tryptophan 6, 72, and 108 to phenylalanine. Once a construct in which only W50 remained was obtained (W@50), mutations changing R83 or R173 to cysteine were created by site-directed mutagenesis as described previously. After each individual mutant was created, the complete sequence of the resulting apo hA-I insert was checked by DNA sequencing to ensure that no other mutations were inadvertently created. The mutant gene products were expressed in *Escherichia coli* BL21/DE3 cells as described elsewhere (*12*). The harvested cells were resuspended in sterile PBS.

Purification and Characterization of Mutant Apolipoproteins. Apo A-I mutants were prepared as described previously (*11*). Briefly, after bacterial cell lysis in sterile buffer, the lysate was suspended in 20 mM sodium phosphate, 150 mM NaCl, 1 mM β-mercaptoethanol, pH 7.4, including a cocktail of antioxidant and protease inhibitors, and the supernatant was purified on a 10 mL Hi-Trap Ni-chelating HP column (Amersham Biosciences). The column was equilibrated with 20 mM sodium phosphate buffer, 500 mM NaCl, 10 mM imidazole, 1 mM β-mercaptoethanol, pH 7.4, before sample loading. The column was then washed by the same buffer containing 100 mM imidazole to remove contaminants. Target protein was eluted by 300 mM imidazole in the same buffer and then dialyzed into desired buffer for future studies. Purified protein was characterized by SDS−PAGE (or Agilent 2100 BioAnalyzer electrophoresis), analytical C18 reversed phase HPLC (Vydac, 218TP104) and electrospray mass spectroscopy. The Agilent BioAnalyzer is a microfluidics "lab-on-a-chip" gel electrophoresis system that provides a read-out of electrophoresed samples analogous to that obtained from a stained SDS−PAGE polyacrylamide gel. Unlike the latter, each sample is electrophoresed individually, and samples are normalized to each other using internal markers and a system peak (for more information see www.agilent.com/chem./labonachip). In all cases, purified proteins were found to be equal to or greater than 90% pure and to contain little or no cystine cross-linked dimer (by electrophoresis and mass spectroscopic determination). Cysteine oxidation was not found to be a problem within 24−48 h in solution. For longer periods, some reducing agent (β-mercaptoethanol, DTT or TCEP) was present in the sample. Extinction coefficients at 280 nm were calculated based on the protein's sequence and used for concentration determinations in 8 M guanidine hydrochloride: 1.07 or 1.12 mL/(mg cm) for wt apo A-I with or without His tag, respectively, and 0.5 mL/(mg cm) for single tryptophan mutants of apo A-I. Unless otherwise indicated, constructs used in the described experiments retained both the histidine tag and the Factor Xa cleavage site. Previous studies have shown that this N-terminal tag has no significant effect on the properties of the protein (*12*, *13*).

Electrospray Mass Spectroscopic Analysis. Mass spectra from a Micromass Q-TOF-2 mass spectrometer were obtained by either the infusion mode or by LCMS. The infusion mode involved delivery of the protein solution using a syringe pump (Harvard Apparatus model 22) at a flow rate of 300 mL/min. The LCMS method used an LC Packings Ultimate liquid chromatograph. The column utilized was a LC Packings Fusica 300 mm PepMap. The flow of 2 mL/min was introduced into the mass spectrometer through the nano-lc inlet. Calculated molecular masses were in agreement with those identified by mass spectrometry.

AEDANS Labeling of Cysteine Containing Mutants. Protein was dialyzed into 50 mM Tris-HCl, pH 7.5, 150 mM NaCl, 5 mM EDTA, 1 mM TCEP (buffer A) and concentrated to about 10 μM. The protein solution was then mixed with an equal volume of the same buffer with 4 M guanidine-HCl (buffer B). A 20-fold excess of 1,5-AEDANS (Molecular Probes) in buffer B was added into the protein to start the labeling reaction. The reaction mixture was kept in the dark under agitation at room temperature for 4 h and then moved to 4 °C for overnight incubation. The extent of the labeling reaction was checked by analytical C18 reverse phase HPLC. A 100 μL aliquot of the reaction was mixed with 6 M guanidine-HCl and injected onto the column. There was a shift in elution time of the protein due to labeling, which allowed the estimation of reaction completion. Once the reaction was more than 90% complete, it was stopped by addition of 10 mM β-mercaptoethanol. Labeled protein was purified by C18 reversed phase HPLC. Fractions containing the labeled protein were lyophilized and stored at −20 °C. The labeling of AEDANS was confirmed by mass spectroscopy.

Factor Xa Cleavage and AEDANS labeling of W@50R83C apo A-I. Proteolytic cleavage of the six-amino acid N-terminal histidine tag was carried out in a 20 mM Tris-HCl buffer, pH 7.4, with 50 mM NaCl and 1 mM TCEP, with a

Factor Xa to protein ratio of 1:25 and reacted at room temperature for 3 h. The reaction was then stopped by adding 10 μM dansyl-Glu-Gly-Arg-chloromethyl ketone (CalBiochem, Inc.), an irreversible factor Xa inactivator. The cleaved protein was purified on a Hi-Trap Ni-chelating column to separate cleaved and His-tagged protein. Further purification was carried out using analytical C18 reverse phase HPLC, and the purified protein was subsequently subjected to AEDANS labeling as described above. After purification of the sample by analytical C18 chromatography, SDS−PAGE showed that the labeled protein was >90% pure. It was not possible to produce cleaved W@50R173C in sufficient quantities for subsequent labeling.

Circular Dichroism (CD). CD spectra were recorded for W@50R83C, W@50R173C, apo Δ(187−243)A-I (minus His tag) and wt apo A-I (minus His tag) on an Olis DSM 1000 CD spectrophotometer (USA). The cells have a path length of 0.02 for far-UV spectra for protein concentrations of 3.4−10.1 μM in 20 mM HEPES, ±1 mM TCEP pH 7.4. A small concentration dependence on the ellipticity was observed for apo A-I and W@50R83C. Spectra were recorded from 260 to 185 nm for far UV in 1-nm steps with a variable scan speed at 22 °C. The molar ellipticity values are calculated according to the following expression: $[\Theta] = (\Theta)(100 \times \mathrm{MRW}/lc)$, where Θ is the ellipticity in millidegrees, MRW is the mean residues molecular weight in grams per mole (116.1 for wt apo A-I and 116.8 for both unlabeled mutants), l is the path length in centimeters, and c is the concentration of the protein in milligrams per milliliter. The value [Θ] has the units of deg cm^2 dmol^{-1}. The calculations of α-helical content are based on the equation $f_H = -([\Theta]_{222} + 2340)/30300$ (*22*).

To monitor thermal unfolding by changes in the far UV CD, the temperature of the monomeric protein (3.4 μM) was increased in steps of 2 °C (through the thermal transition range) or 4 °C (below the thermal transition) at an average rate of 0.3 °C/min. The sample equilibrated at each temperature for approximately 7−9 min, and 3 scans were recorded from 215 to 225 nm, which were subsequently averaged (total time at each temperature was <14 min). The unfolding profiles were normalized and a van't Hoff analysis was used to obtain the unfolding temperature, T_m, and enthalpy, ΔH_{vH}.

Differential Scanning Calorimetry (DSC). All DSC scans were performed with an N-DSC II differential scanning calorimeter (Calorimetry Sciences Corp.). Lyophilized wt apo A-I (minus His tag) or apo Δ(187−243)A-I (minus His tag) were dissolved in 6 M guanidine-HCl to approximately 0.2 mg/mL and dialyzed extensively against 10 mM sodium phosphate, pH 7.2 at 4 °C. The dialysate was filtered through a 0.22 μM syringe top filter and degassed. It was loaded into the DSC cells and scanned up and down from 0 to 110 °C at 1 °C/min several times to condition the cells and establish the buffer baseline. Protein solution was then degassed and loaded into the sample cell and scanned up to 110 °C at the same scan rate. Scans of apo Δ(187−243)A-I were obtained in a similar manner in 20 mM sodium phosphate, pH 7.4. The concentrations of protein used in the DSC scans shown in Figure 7 are both 0.16 mg/mL. A repeat scan of the same protein sample was performed to determine reversibility of unfolding, and both were found to be largely reversible. Exact concentration of protein in the cell was determined by absorbance at 280 nm using an extinction coefficient of 1.12 (mg/mL)$^{-1}$cm^{-1} for wt apo A-I and 1.31 (mg/mL)$^{-1}$ cm^{-1} for apo Δ(187−243)A-I. DSC data were exported as ASCII files and analyzed using MicroCal Origin 5.0 for DSC software.

Fluorescence Measurements. Experimental Methods. Steady-state fluorescence measurements were carried out at 20 °C on an ISS PC1 photon-counting spectrofluorometer, using a band-pass of 3 nm on both the excitation and the emission monochromators. All fluorescence spectra were recorded on monomeric concentrations of protein at 5 μM in 50 mM Tris, pH 8.0, 0.1 M NaCl, and 1 mM DTT. When present, the urea concentration was 5 M. All emission spectra were background subtracted with solutions in which proteins were omitted and corrected for variation of the detector system with wavelength. Quantum yields of Trp50 in W@50R83C and W@50R173C apo A-I mutants were determined with excitation at 295 nm by the comparative method (*23*) using corrected emission spectra and L-tryptophan as the standard as previously described (*24*). Measured quantum yields were used in the calculation of R_0, the Förster critical distance (eq 3, see below).

Fluorescence intensity decays were measured at 20 °C in the time domain with an IBH 5000 photon-counting lifetime system equipped with a very stable flash lamp operated at 40 kHz in 0.5 atm of hydrogen. For FRET measurements, the donor was tryptophan 50 and the acceptor was the extrinsic fluorophore AEDANS covalently linked to the single Cys83 or Cys173 of W@50R83C and W@50R173C. The excitation wavelength was 295 nm and the emission wavelength was 333 nm for donor tryptophan. Intensity decays of the donor from the donor-alone and donor−acceptor samples were collected into 1024 channels of a multichannel analyzer (PCA3) under identical experimental conditions and were corrected for background signals using an identical solution in which the protein was omitted. These decays were used to calculate the distribution of intersite distances between donor and acceptor as in previous work (eqs 2 and 4, see below) (*25*).

FRET Theory and Analytical Methods for Determination of Intersite Distances. The physical basis for determination of an ensemble of intersite distances by FRET has been previously described (*26*−*28*). We summarize here the time-domain procedure used in the present analysis to facilitate discussion. Donor intensities, in the absence of energy transfer, are fitted by convoluting the observed lamp profile with a multiexponential function of the form

$$D(t) = \sum_i \alpha_{Di} \exp(-t/\tau_{Di}) \quad (1)$$

where α_{Di} is the fractional amplitude associated with the lifetime τ_{Di} for the ith component. In the presence of Förster resonance energy transfer, the distance-dependent donor intensity decay of a donor−acceptor pair separated by a given distance r is given by

$$I_{DA}(r,t) = \sum_i \alpha_{Di} \exp[-(t/\tau_{Di}) - (t/\tau_{Di})((R_0/r))^6] \quad (2)$$

where R_0 is the Förster critical distance at which the energy transfer efficiency is 0.5. R_0 is experimentally derived for

each donor−acceptor pair from

$$R_0 = 0.211[\kappa^2 n^{-4} Q_D J(\lambda)]^{1/6} \text{ (in Å)} \quad (3)$$

where wavelength is expressed in nanometers, κ^2 is the orientation factor, n is the refractive index of the medium, Q_D is the quantum yield of the donor in the absence of acceptor, and $J(\lambda)$ is the spectral overlap integral. $J(\lambda)$, which quantifies the degree of spectral overlap between the donor emission and acceptor absorption, is calculated from the respective corrected and normalized spectra of the donor and acceptor. It is common to use the dynamic averaging value 2/3 for κ^2, but whether this assumption is valid for any FRET study should be determined on a case by case basis (*28*). In the present studies, it is a reasonable assumption. Chromphores that have mixed polarizations and are characterized by multiple dipole transitions across the absorption band can have a narrow κ^2 range (*29*), and when the acceptor (not donor) chromophore exhibits this property, reduction of the κ^2 ranges toward 2/3 occurs (*30*). AEDANS, the acceptor used in the present studies, is a close structural homologue of the dansyl moiety (both are 5 substituted 1-sulfonyl-naphthalenes), which is known to exhibit mixed polarizations across the absorption band (*29*).

The observed donor intensity decay may be treated in the most general case as an ensemble of donor−acceptor pairs and is given by the average of the individual decays weighted by the distance probability distribution [$P(r)$] of the donor−acceptor pair (*26*),

$$I_{DA}(t) = \int_0^\infty P(r) I_{DA}(r,t) dr \quad (4)$$

The probability distribution is usually assumed to be a Gaussian with a mean distance $\langle r \rangle$ and half-width (hw) of the distribution. The standard deviation (σ) of the Gaussian is related to the half-width by hw = 2.354σ.

The distributions of the distances between W@50 and Cys83 and between W@50 and Cys173 were calculated using the program CFS_LS/GAUDIS, using data obtained from corrected donor fluorescence decays and experimental values of R_o separately determined for each mutant. The reduced chi squares ratio (χ_R^2) and an analysis of the dependence of this ratio on the mean distance and the half-width were used to judge goodness of fit for the distribution and determine the upper and lower estimates of the mean distance and the half-width at the 68% confidence level (*26*, *28*).

RESULTS

Expression, Purification, and Physical Characterization of apo A-I Recombinant Proteins. The construction and expression in *E. coli* of wt apo A-I, W@50R83C, and W@50R173C were made possible using the gene for full-length mature human apo A-I containing an N-terminal His-tag and Factor Xa cleavage site. The general methods for mutagenesis, expression, and purification have been previously described (*11*, *12*, *13*). Mutagenesis was performed in a stepwise fashion. First, the single tryptophan 50 mutant was constructed by replacing tryptophans at positions 8, 72, and 108 with phenylalanine. A similar triple substitution mutant, containing an N-terminal prosequence, was constructed by Davidson et al. (*14*), and we have adopted their nomenclature for this substitution pattern, i.e., W@50. From W@50, two new mutants were constructed, each with an arginine to cysteine replacement at either arginine 83 (W@50R83C) or arginine 173 (W@50R173C).

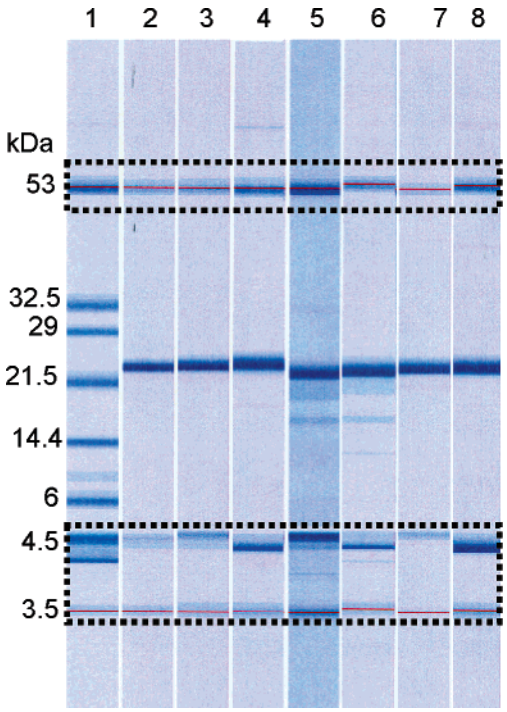

FIGURE 1: Electrophoretic analysis of purified proteins. Lane 1, MW standard markers; lane 2, wt apo A-I; lane 3, W@50R83C; lane 4, W@50R83C-AEDANS; lane 5, W@50R83C (minus His-tag); Lane 6 W@50R83C-AEDANS (minus His-tag); lane 7, W@50R173C; lane 8, W@50R173C-AEDANS. Proteins were analyzed by the Agilent Bioanalyzer. Dashed boxes surround the internal markers (at 53 and 3.5 kDa) and system peaks (4.5 kDa), respectively (see Experimental Procedures for details).

Purified proteins were labeled with the extrinsic fluorescent probe iodo-AEDANS and repurified by reversed phase HPLC. Purity and stoichiometric labeling was confirmed by electrophoresis (Figure 1, Table 1) and mass spectroscopy (Table 1). Both AEDANS-labeled proteins were estimated to be greater than 99% pure by densitometric analysis of the electrophoresis profile, and singly labeled by AEDANS by mass spectroscopy. His-tag minus W@50R83C and W@50R83C-AEDANS were also prepared for confirmatory analysis (Table 1). As shown in Tables 1−4 (discussed below), no discernible differences were observed between the plus and minus His-tag constructs.

Significant physical characterization of single tryptophan mutants has been conducted previously, which showed that W@50 has secondary structure, stability, and lipid binding properties similar to wild-type apo A-I (*14*). As shown here, a further cysteine replacement does not cause significant structural perturbation. The W@50R83C and W@50R173C constructs have similar secondary structures to wild-type apo A-I, based on far-UV circular dichroism (Figure 2 and Table 1). After labeling with AEDANS, stability was assessed by monitoring thermal unfolding in the far UV CD (Figure 3 and Table 1). Midpoint unfolding temperatures (T_m) of labeled mutants were found to be within a few degrees of wild-type apo A-I, and van't Hoff enthalpies (ΔH_{vH}) of unfolding were also similar to wild type. T_m and ΔH_{vH} of wild-type apo A-I were very similar to those reported previously (*18*, *21*).

Table 1: Analysis of Protein Purity, Identity, and Stability of wt apo A-I and Mutants

protein	% purity[a]	% helix	mass:[b] experimental / calculated	T_m[c] / ΔH_{vH} (kcal/mol)
wt apo A-I	95	50.8		61.3 ± 0.8 °C[d]
				59.4 ± 0.3 °C[e]
				39.3 ± 4.0[d]
				39.1 ± 1.5[e]
W@50R173C[d]	93	48.4 ± 1.0		
W@50R173C-AEDANS[d]	99		29625	61.7 ± 0.6 °C
			29624	31.4 ± 1.7
W@50R83C[d]	97	52.5 ± 3.5		
W@50R83C-AEDANS[d]	99		29624	58.6 ± 0.4 °C
			29624	31.5 ± 1.2
W@50R83C-AEDANS[e]	90		28215	
			28215	

[a] Based on Bioanalyzer analysis; see Figure 1. [b] Determined by mass spectrometry. [c] Determined by CD measurements; see Figure 3. [d] Measurement on plus His-tag construct. [e] Measurement on minus His-tag construct.

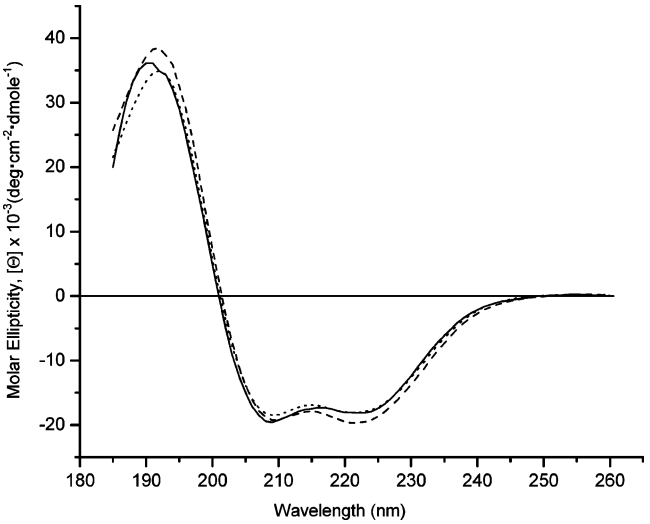

FIGURE 2: Far-UV circular dichroism of wt apo A-I and W@50 mutants. Wt apo A-I, solid line, 8.6 μM; W@50R83C, dashed line, 8.1 μM; W@50R173C, dotted line, 5.1 μM.

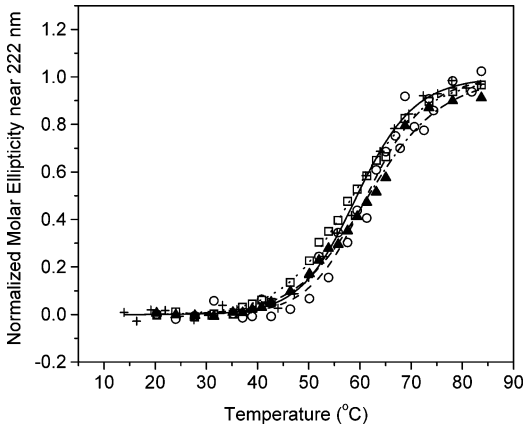

FIGURE 3: Thermal unfolding of wt apo A-I and its AEDANS labeled W@50 apo A-I mutants. Wt apo A-I/minus His tag, (+, solid line); wt apo A-I/plus His tag (○, dashed line); W50@R83C (□, dotted line); W@50R173C (▲, dash−dotted line); as detected by CD. Each point represents the average of normalized data collected from 222 to 224 nm. The lines represent the van't Hoff fit from which the T_m and ΔH_{vH} were obtained (given in Table 1).

The fluorescence emission properties determined from the corrected spectra of W@50R83C and W@50R173C are indistinguishable, as summarized in Table 2. The emission maxima (λ_{max}) are 334 and 333 nm, and the quantum yields

Table 2: Steady-State Fluorescence Properties of Monomeric W@50 apo A-I Single Tryptophan Mutants

protein	condition	λ_{max}(nm)	quantum yield
W@50R83C	native	334	0.23
W@50R83C	+urea	349	0.14
W@50R83C[a]	native	335	0.22
W@50R83C[a]	+urea	348	0.11
W@50R173C	native	333	0.22
W@50R173C	+urea	349	0.12

[a] Measurements made on the minus His-tag construct.

Table 3: Fluorescence Lifetimes of Monomeric W@50 apo A-I Single Tryptophan Mutants

		fluorescence lifetimes (ns)			
sample	condition	τ_1	τ_2	τ_3	$\langle\tau\rangle$
W@50R83C	native	8.32(0.08)[a]	2.86(0.47)	0.78(0.45)	4.10
W@50R83C	+urea	7.86(0.06)	2.58(0.50)	0.67(0.44)	3.51
W@50R83C[b]	native	8.50(0.07)	2.86(0.34)	0.64(0.59)	4.10
W@50R83C[b]	+urea	8.16(0.05)	2.68(0.46)	0.66(0.49)	3.48
W@50R173C	native	8.42(0.07)	3.29(0.38)	0.91(0.55)	4.08
W@50R173C	+urea	7.92(0.06)	2.72(0.43)	0.77(0.51)	3.52

[a] The numbers in parentheses are the fractional amplitudes (α_i) associated with the individual lifetime components τ_i. $\langle\tau\rangle$ is the intensity-weighted mean lifetime calculated from: $\langle\tau\rangle = \sum\alpha_i\tau_i^2/\sum\alpha_i\tau_i$. [b] Measurements made on the minus His-tag construct.

are 0.23 and 0.22, respectively. The values of both the emission maxima and associated quantum yields are consistent with each other and indicate that in the folded state, W@50 is substantially shielded from solvent. These λ_{max} values for W@50 are 4−5 nm shorter than the value previously reported, which was obtained from an uncorrected emission spectrum (*14*). In the presence of 5 M urea, the λ_{max} of both mutants becomes red-shifted to 349 nm, and their respective quantum yields are reduced to 0.14 and 0.12. These results are consistent with unfolded proteins where W@50 is exposed to the solvent. The steady-state fluorescence results indicate that the substitutions of Arg83 and Arg173 by cysteine do not alter the local structural environment of apo-A1 in the region of W@50. Collectively, the data summarized in Tables 1 and 2 indicate that no significant structural perturbations occur in apo A-I with the mutations described or subsequent AEDANS labeling of cysteine.

Time-Domain Fluorescence Measurements. The intensity decays of W@50 in all mutants could not be fitted with a monoexponential function but could be fitted with three

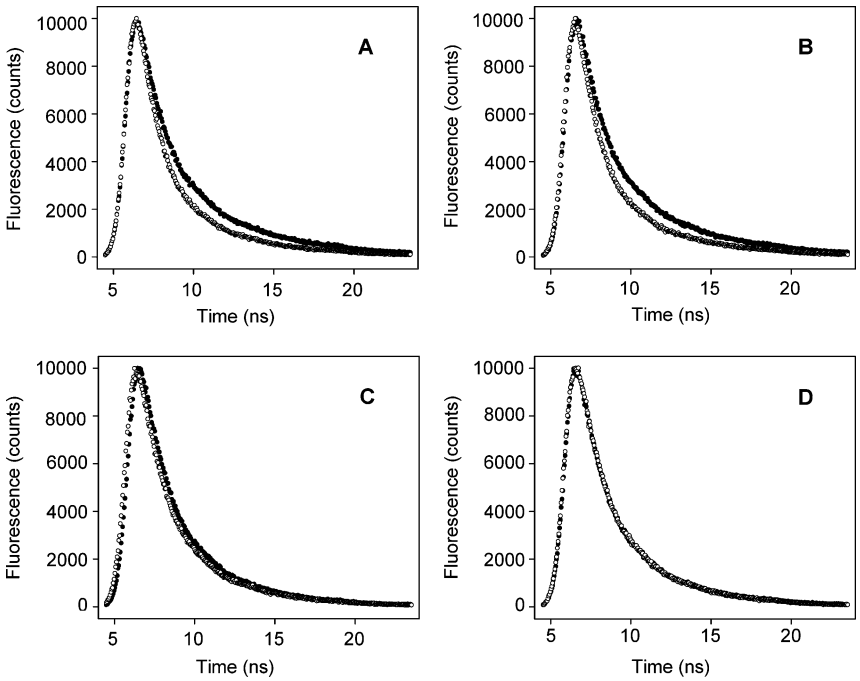

FIGURE 4: Fluorescence intensity decays of apo A-I W@50 apo A-I mutants with and without labeled AEDANS. (A) Native W@50R83C. (B) Native W@50R173C. (C) W@50R83C + urea. (D) W@50R173C + urea. (●): decay in the absence of an acceptor; (○): decay in the presence of an acceptor (AEDANS linked to cysteine).

exponentials yielding three lifetimes (Table 3). Three lifetimes are commonly observed in proteins containing single tryptophans and have been reported before for the single tryptophan apo A-I mutants (*14*). The intensity-weighted mean lifetimes are in the range 4.08−4.10 ns, and the corresponding mean lifetimes of the mutants in urea are 3.48−3.52 ns. The very narrow range of the mean lifetimes suggests very similar local environment for W@50 in the mutants.

Figure 4 shows the intensity decays of W@50 in W@50R83C and W@50R173C (donor only) and with labeled AEDANS (donor−acceptor). In the folded state, the decay in the donor−acceptor sample is faster than in the donor-only sample (compare closed symbols to open symbols in the upper panels A and B). This is evidence of energy transfer from the donor to the acceptor. In 5 M urea (lower panels C and D), the two decay profiles are superimposable, indicating negligible energy transfer between the two fluorophores when the protein is unfolded.

Intensity decay data showing energy transfer are fit to a triexponential function with a single Gaussian function for $P(r)$, (eq 4 in Experimental Procedures). Figure 5 illustrates the best fit curves for W@50R83C-AEDANS. The distribution of the intersite distances between W@50 and Cys83 was calculated from the best fit of the data and is displayed in Figure 6. Also shown is the distribution of the distances between W@50 and Cys173. These distance parameters are summarized in Table 4.

The mean distances between W@50 and C83 and between W@50 and C173 are 21.4−22.3 Å (representing ± His tag constructs) and 19.2 Å, respectively. The experimental value of the Förster distance (R_o) for the donor−acceptor pair used in this study, 23.7−24.2 Å, is optimal for determination of these intersite distances, since it is in this range of distances that energy transfer will be easily detected. The half-widths of the distributions are 3.7−5.6 Å. Since the half-width is

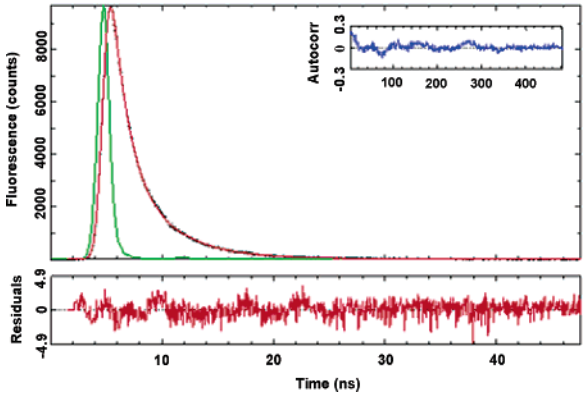

FIGURE 5: An analysis of energy transfer from donor tryptophan in W@50R83C-AEDANS to the acceptor. As an example, data taken from Figure 4A are shown here. The sharp peak (green) on the left is the excitation light pulse. The donor intensity decay in the presence of acceptor (broad peak on the right, black points) was fit (red line through points) to eq 4 (see Experimental Procedures) with a single Gaussian as $P(r)$ and a sum of three exponential terms for $I_{DA}(r,t)$ (eq 2). The residual plot of the fit is shown in the lower panel across the figure, and the autocorrelation plot is shown as an inset at the upper right corner. The best-fit data from this analysis were used to calculate the distribution of the intersite distances between W@50 and the acceptor AEDANS attached to C83.

related to the standard deviation of the Gaussian, a half-width in the range 4−6 Å is suggestive of little structural dynamics between the helices where the three residues (W50, C83, and C173) are located. This interpretation will be discussed below in further detail. Upon denaturation of the sample in urea, the mean distances increase, indicating a decrease in energy transfer, as expected. The concomitant increases in the half-width reflect an increase in random motions of the polypeptide.

The relatively narrow half-widths of the single-distribution fits support a discrete structure for lipid-free apo A-I. Since this conclusion is at odds with previous data suggesting a

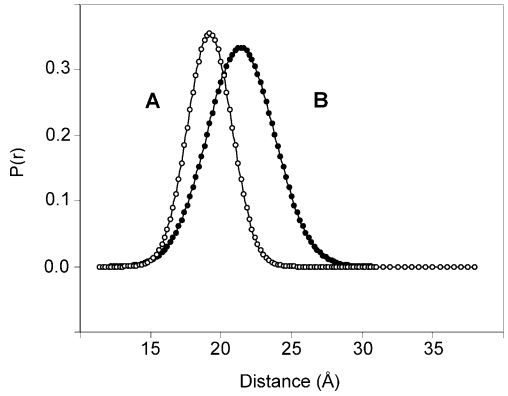

FIGURE 6: Area-normalized distributions of intersite distances between W@50 and C173-AEDANS in W@50R173C (A) and between W@50 and C83-AEDANS in W@50R83C (B).

dynamic equilibrium between a closed bundle conformation and an open hairpin conformation (*13*), we also investigated whether the FRET data could be better described by two distributions of the intersite distances, which would be compatible with a dynamic interchange between these two extremes in conformation. This analysis was accomplished by using two Gaussian functions for $P(r)$ in the calculations. These results are included in Table 4. Because of the inverse sixth power dependence of FRET on the distance, the distance distribution is heavily weighted toward short distances. Therefore, it is not surprising that the short-distance distributions are similar to the single distributions in both the mean distance and the half-width. The long-distance distribution is considerably broader than the short-distance distribution for W@50R83C (a 2-fold increase in half-width), but the reverse was found for W@50R173C. In fact, the half-width of 0.5 Å is not physically meaningful and is indicative of a poor model for fitting. Further evidence for this conclusion is the mean distance of 80 Å recovered from the long-distance distribution, which is also not physically meaningful. Such a long distance of 80 Å is $> 2R_o$ for the tryptophan−AEDANS pair and would not be resolvable. For both of the two-distribution fits, there is no improvement in the fitting statistics (χ_R^2) over the single-distribution fits. While it is not possible to unequivocally rule out the bimodal fits, taken together, these considerations lead to the conclusion that the present FRET results are most consistent with a single distribution (and do not support a bimodal distribution) for the separations between W@50 and C83 and C173.

Differential Scanning Calorimetry. The data presented thus far are consistent with a discrete structure for apo A-I (single distribution function of relatively narrow half-width). However, this interpretation is not consistent with the widely held view that lipid-free apo A-I is a molten globule (*5*, *21*, *31*). The first and still the most direct evidence suggesting a molten globule state was published by Gursky and Atkinson in 1996, based on DSC of apo A-I thermal unfolding (*8*). This is the best approach to obtain the necessary thermodynamic parameters required to identify the presence of an equilibrium state such as the molten globule (*32*). We decided to look at this issue again with a more sensitive DSC instrument and at an apo A-I concentration where the monomer is the predominant species (0.16 mg/mL), representing a 10-fold lower concentration than the lowest used in the earlier study.

Shown in Figure 7 are the DSC data obtained for recombinant wt apo A-I under solution conditions similar to those reported earlier (*8*). Thermodynamic analysis of the endotherm indicates the monomer unfolds in two steps represented by two two-state transitions (see Table 5). The ratio $\Delta H_{vH}/\Delta H_c = 0.50$, not 0.16 as obtained previously. The van't Hoff enthalpy, $\Delta H_{vH} = 41.8$ kcal/mol, compares well to the spectroscopically derived value (Table 5) and the earlier DSC value (*8*). The presence of two two-state transitions suggests that apo A-I unfolding proceeds through a single intermediate, i.e., a three-state unfolding model. Thermal unfolding was also monitored by far UV CD, and the normalized data are shown in Figures 3 and 8. The data can be fit equally well to either a two- (Figure 3) or a three-state (Figure 8) model.[2]

In our 1998 publication (*12*), we compared the structure and stability of full-length apo A-I to a C-terminal deletion mutant, apo Δ(187−243)A-I. We concluded that the folded core of apo A-I is contained within the N-terminal 1−186 residues due to the similarities in a variety of physical and spectral properties, including structural stability and the near-UV CD for the two proteins. This viewpoint has subsequently been reinforced by others (*21*). In fact, a CD analysis of the thermal unfolding of a similar C-terminal construct led to the suggestion that removal of the C-terminus increases the cooperativity of the remaining structure (*21*).

An increase in cooperativity would be readily detected by DSC, which also allows for a quantitative analysis. DSC was, therefore, performed on apo Δ(187−243)A-I and the resulting DSC and CD curves are shown in Figures 7 and 8, respectively. The DSC transition fits well to a single two-state transition for the monomer, as shown. The ratio $\Delta H_{vH}/\Delta H_c = 1.0$ (derived from a single non-two-state fit; fit not shown), which is equivalent to a two-state fit. This result is consistent with a single, discrete, cooperative domain. For comparison, the CD data is also shown fit to a two-state transition (Figure 8). The ΔH_c for full-length wt apo A-I and apo Δ(187−243) A-I are essentially the same (Table 5), which is consistent with our earlier suggestion that the folded core of the protein resides within the first 186 residues.

DISCUSSION

The DSC and FRET data reported here are consistent with a structure for lipid-free apo A-I that is both discrete, and as discussed below, globular. These data are inconsistent with earlier reports that the structure is conformationally dynamic and/or exists as an ensemble of conformations, typical of a molten globule (*8*, *13*). Possible reasons for the lack of correspondence with earlier data will be posed.

DSC Analysis of Molten Globules: Background. The lack of a cooperative structure is a hallmark of the molten globule state and was originally thought to be a universal feature of molten globules since early on species identified as such had no detectable unfolding transition (*33*, *34*). However, there

[2] For noncalorimetrically derived unfolding data, it is not unusual to find that the number of experimental points is sometimes insufficient to distinguish between unfolding models. Normally, we would use the simplest model that fits the data to obtain thermodynamic parameters, and in the past we have used a thermodynamic two-state fit to obtain ΔG_{H_2O} values (*11*, *12*), as have all others reporting such values for apo A-I. A three-state fit is shown simply to illustrate that the CD data are not inconsistent with it.

Table 4: Intersite Distance Parameters for Monomeric AEDANS-Labeled W@50 apo A-I Single Tryptophan Mutants

protein	conditions	R_0 (Å)	mean distance (Å)	half-width (Å)	χ_R^2
W@50R83C					
single-distribution fit	native	24.2	21.4(−0.8, +1.0)[a]	5.6(−0.3, +0.2)[a]	1.18
two-distribution fit			21.1(79%)[b]	6.3	1.19
			30.5(21%)	11.1	
single-distribution fit	unfolded/+urea	20.1	35.2(−1.2, +1.5) [a]	8.9(−0.5, +0.6)[a]	1.17
W@50R83C[c]					
single-distribution fit	native	24.1	22.3(−0.9, +0.7)[a]	5.0(−0.4, +0.3)[a]	1.20
single-distribution fit	unfolded/+urea	19.8	29.3(−1.4, +1.5)[a]	10.6(−0.6, +0.7)[a]	1.26
W@50R173C					
single-distribution fit	native	23.7	19.2(−0.9, +0.9)[a]	3.7(−0.4, +0.2)[a]	1.21
two-distribution fit			22.2 (56%)[b]	4.1	1.23
			80.0 (40%)	0.5	
	unfolded/+urea	19.7	no FRET detected	no FRET detected	NA

[a] Numbers in parentheses are the lower and upper 68% confidence (one standard deviation) estimates of the fitted mean distance and half-width. [b] Number in parentheses given with each of the two mean distances (from the two-distrubution fits) are the amplitudes associated with the individual distances. [c] Measurements made on the minus His-tag construct.

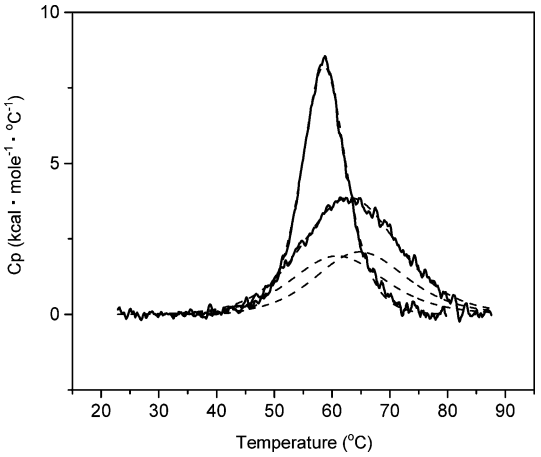

FIGURE 7: Differential scanning calorimetry of wt apo A-I and the C-terminal truncation mutant, apo Δ(187−243)A-I (both in the absence of His tags). For purposes of comparison, the heat capacity profiles of each protein (normalized to the monomeric concentration) are superimposed. Data are shown in solid lines and fitted curves are shown in dashed lines. The single curve centered near 59 °C is for apo Δ(187−243)A-I and is fit with a single two-state unfolding model. Wt apo A-I is broader and centered near 63 °C. It is best fit to two two-state transitions, as shown. The thermodynamic parameters associated with these fits are given in Table 5.

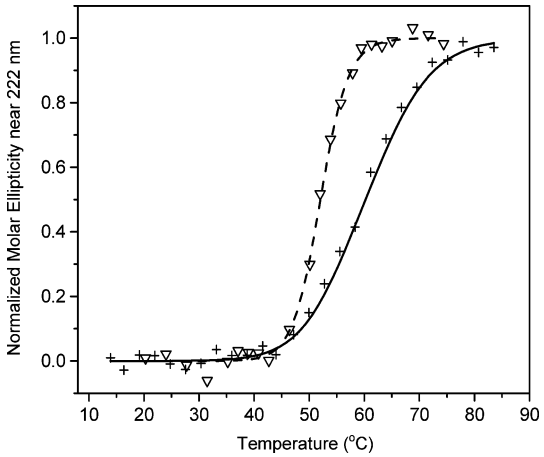

FIGURE 8: Thermal unfolding of wt apo A-I and the C-terminal truncation mutant, apo Δ(187−243)A-I. Wt apo A-I/minus His tag, (+, solid line); apo Δ(187−243)A-I/minus His tag (▽, dashed line); as detected by CD. Each point represents the average of normalized data collected from 222 to 224 nm. The data for wt apo A-I is the same as that shown in Figure 3 and is repeated here for clarity and for direct comparison to the mutant. The lines represent the van't Hoff fit to a three-state fit for apo A-I (for comparison to the two-state fit shown in Figure 3) and a two-state fit for apo Δ(187−243)A-I. The T_m and ΔH_{vH} obtained from these fits (two-state only) are given in Table 5.

are now many examples of molten globular structures that show cooperativity (*32*, *35*, *36*). Some degree of cooperativity is implicit in the ability to detect (either spectroscopically or by calorimetry) unfolding induced by heat or denaturants. Arai and Kuwajima have reviewed the cooperativity of molten globules in detail (*32*). The degree of cooperativity can only be determined by a calorimetric analysis, by comparison of the van't Hoff and calorimetric enthalpies. A discrete structure will unfold through one or more two-state transitions. This ratio is 1 for a single two-state transition and 0.5 for a three-state transition (or two two-state transitions). The molten globule will not exhibit this level of cooperativity since it is an ensemble of structures with different energies and different amounts of residual structure, even though they may share a common structural feature (*37*). A statistical thermodynamic formalism for this concept shows that if there are as few as 2 to 3 independent residual structural elements that must unfold during the transition between the molten globule and the fully unfolded denatured state, the ratio of the van't Hoff to calorimetric enthalpy will be much lower than 0.5 and will be less cooperative than either a two-state or three-state transition (*38*).

New Results Lead to Different Conclusions: Why? On the basis of the DSC data presented here, there is good reason to believe that apo A-I exhibits a discrete, compact structure. The low thermodynamic stability of apo A-I is not at odds with this interpretation nor is the vast majority of the experimental data that exist for apo A-I, with the exception of the earlier DSC study of Gursky and Atkinson (*8*), and our own results indicating dynamic conformational heterogeneity. We drew this conclusion from a van Holde-Weishet analysis of sedimentation velocity data (*13*). A likely explanation for the inconsistency between the results from this earlier study and the present is found in the different techniques used. The protein is subjected to an external centrifugal force during collection of the sedimentation velocity data. On hindsight, it seems likely that the relatively low stability of apo A-I is not sufficient to withstand such forces. However, since the changes are subtle and reversible

Table 5: Thermodynamic Parameters Obtained from Fits of wt apo A-I and apo Δ(187−243)A-I Thermal Unfolding

	CD[a]		DSC		
protein	T_m	ΔH_{vH} (kcal/mol)	T_m	ΔH_{vH} (kcal/mol)	ΔH_c (kcal/mol)
wt apo A-I				single non-two-state	
	59.4 ± 0.3 °C	39.1 ± 1.5	63.29 ± 0.04 °C	41.8 ± 0.2	83.8 ± 0.4
				two two-state[b]	
			61.2 ± 0.3 °C	41.4 ± 0.8	41.4 ± 0.8
			65.2 ± 0.2 °C	43.4 ± 0.8	43.4 ± 0.8
apo Δ(187−243)A-I				single two-state[b]	
	52.3 ± 0.3 °C	83.7 ± 8.2	58.65 ± 0.01 °C	84.7 ± 0.1	84.7 ± 0.1

[a] Parameters are obtained from a two-state fit of the data. Parameters obtained from a three-state fit are not given because they are not statistically significant. [b] In a two-state fit, ΔH_{vH} and ΔH_c are contrained to be the same.

and the protein does not denature during the course of the experiment, this dynamic behavior has gone undetected by other means of analysis.

Second, why do these new DSC results differ from the earlier DSC study? Using the best instrumentation available at the time, apo A-I unfolding was shown to be of very low cooperativity, as evidenced by the ratio of the van't Hoff to calorimetric enthalpy, 0.16, where $\Delta H_{vH} = 32.5 \pm 5$ kcal/mol and $\Delta H_c = 200 \pm 20$ kcal/mol (*8*). In further support of this conclusion were far-UV CD spectra taken over the thermal unfolding transition. These did not show an isochromatic point, consistent with a low cooperative, non-two-state unfolding. In fact, the data we present is also consistent with this CD result since an isochromatic point would not be observed for a three-state unfolding transition, unless the two transitions were widely separated in temperature.

The primary caveat in the earlier data was the relatively high concentration of apo A-I needed to obtain a detectable DSC signal, the lowest being 1.7 mg/mL (8), a concentration in which apo A-I exhibits high-order oligomers.[3] Although convincing data were presented that the oligomers of apo A-I present at these concentrations dissociated below the temperature of the unfolding endotherm, the most reasonable explanation for the lack of correspondence between our data and those is the relative insensitivity of the instrumentation used in the early work.

Structural Interpretation of DSC Data. The unfolding of full-length apo A-I is best represented by two two-state transitions. There may be several plausible structural interpretations consistent with this thermodynamic analysis. For instance, the two transitions may represent the unfolding of two *folded* domains. Since the number of transitions is reduced to one for the C-terminal truncation mutant apo Δ(187−243)A-I, it is tempting to equate the two transitions observed in full-length apo A-I with the unfolding of an N-terminal (residues 1−186) and C-terminal (residues 187−243) domain. We have also observed a single, two-state unfolding transition for a C-terminal truncation mutant of mouse apo A-I (residues 1−216) (*39*). Attributing the two transitions to these domains cannot be ruled out, but this explanation seems unlikely. It is possible to roughly correlate the unfolding enthalpy to the size of the cooperative unfolding unit and in this case, the ΔH_c for each of the two transitions in the full-length protein are very similar, while the size of the two presumptive domains are not (186 versus 56 residues). In fact, the ΔH_c for apo Δ(187−243)A-I is essentially the same as the ΔH_c for the combination of both transitions in full-length apo A-I, while one might expect it to be close to ΔH_c for only one of the two transitions. Despite the foregoing discussion, the unfolding of 2-folded domains remains a possible explanation for the two transitions observed in the full-length apo A-I, even though the exact identity of the domains cannot be determined by the present studies. An alternative explanation for the two transitions observed for full-length apo A-I is that they represent the sequential unfolding of the protein, which undergoes a conformational change in the first step to a different conformation that unfolds in the second.

Structural Interpretation of FRET Distances: A Model for apo A-I. If one accepts the possibility that the apo A-I structure is discrete, then it is reasonable to build a model structure that is consistent with the measured FRET distances or to compare the FRET distances with an existing model. Given the limited number of distances, we have done the latter. Figure 9 shows the hypothetical globular helix bundle and elongated helical hairpin structures from which distances were calculated and compared with those derived from the experimental FRET measurements. The crystal structure of tetrameric apo Δ(1−43)A-I (*10*) has allowed for the construction of these models for a monomeric helical bundle and hairpin. These structures and the rationale for proposing them have been presented previously (*2*, *9*, *13*). A key rationale for using the apo Δ(1−43)A-I crystal structure to construct novel structures for an apo A-I helical bundle and hairpin is the reasonable assumption that the specific helical pairs observed in the crystal structure are preferred because they have intrinsic thermodynamic stability, and so alternative three-dimensional forms also containing these helical pairs may exist.

While represented schematically here as cylinders, the published crystallographic coordinates were used to calculate hypothetical distances for each model (*10*), which are given in Table 6. Because of the overall curvature of this tetrameric helical bundle (see ref *40*), the measured distances should be viewed only as approximations that are no more or less valid than a helical model designed de novo. Because it is impossible to know how the side chains are oriented in solution, the measurements are given from C_α to C_α, which will necessarily underestimate the distance between donor and acceptor. Even with these limitations, the differences between the calculated distances for the globular helical bundle and the elongated helical hairpin models are so large that it is possible to distinguish between the two structural models in

[3] In 1999, Suurkuusk and Hallén published the DSC of apo A-I at the somewhat lower concentration of 1 mg/mL (*49*). This concentration, nevertheless, will exhibit high-order oligomers. They report a similar lack of cooperativity for apo A-I thermal unfolding as shown by Gursky and Atkinson (*8*).

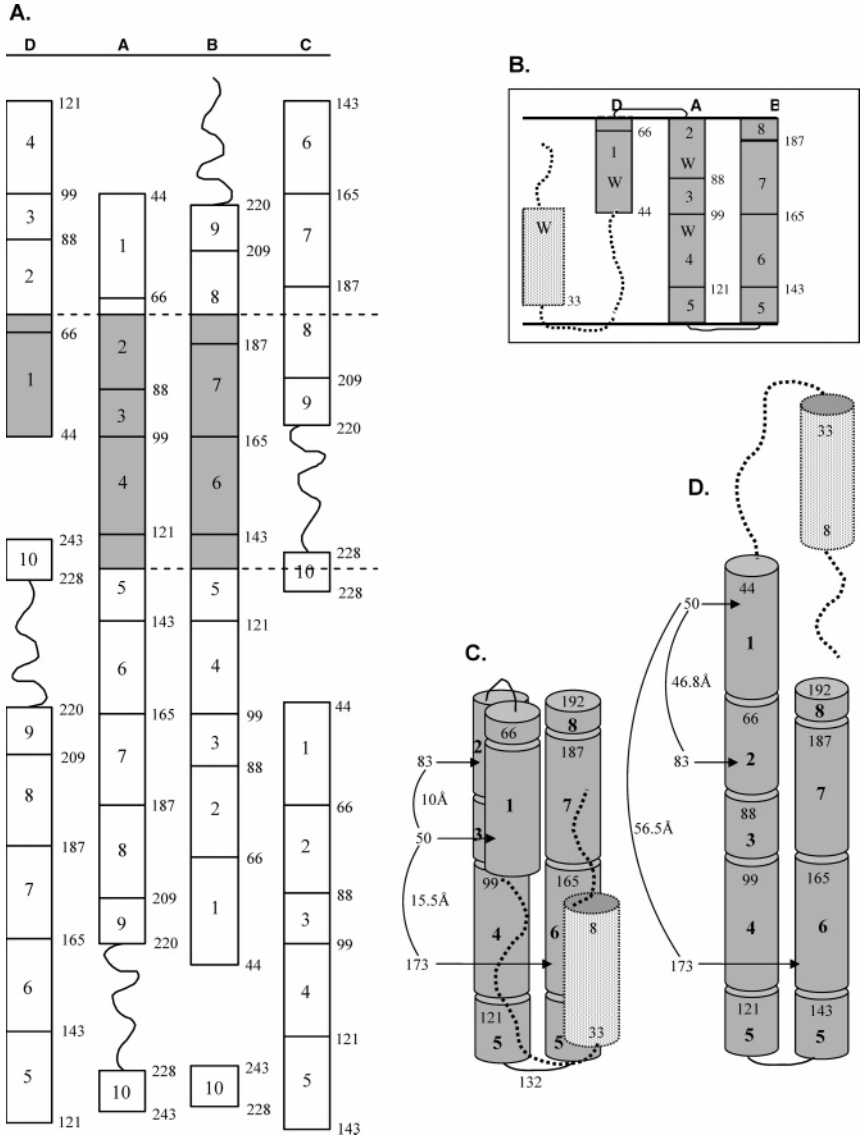

FIGURE 9: Schematic drawings of structural models for apo A-I. (A) Simplified helical net diagram of the intermolecular associations and alignment of protein molecules A, B, C, and D found in the crystal structure of tetrameric apo Δ(1−43)A-I, a mutant of apo A-I missing residues 1−43 (*2*, *10*). The diagram illustrates the specific helix-helix pairings along the length of each monomer within the tetramer. The nomenclature for helices (1−10) and monomers (A, B, C, D) is found in ref 9. The lengths of all strands, helical and nonhelical, are roughly to scale according to the crystal structure. (B) Helical net diagram of the proposed helical bundle structure for monomeric apo A-I, derived from the intermolecular helical pairs found in tetrameric apo Δ(1−43)A-I. Dashed lines that extend through structure in panel A indicate which portion of the tetramer structure (shaded helices) is used to construct the hypothetical monomeric structure. Implicit in this transformation are the following assumptions: (i) that the structure of the central residues 44−187 are largely unchanged; (ii) the structure of residues 193−243 in lipid-free apo A-I are not critical to the integrity of the helical bundle. Residues 8−33 have been modeled as helical based on a secondary structure analysis (*46*) and NMR of an apo Δ(187−243)A-I deletion mutant (*47*). The nonhelical regions of 1−33 are assumed to be in an extended conformation (*48*) and lengths are modeled roughly to scale. The secondary structure of residues 193−243 found in the apo Δ(1−43)A-I crystal structure were not used and are absent in the monomeric models of apo A-I shown in panels B, C, and D since there is experimental evidence that in apo Δ(1−43)A-I these residues adopt the lipid-bound conformation of apo A-I (*11*). The letter W denotes the position of native tryptophans at 8, 50, 72, and 108. (C) Three-dimensional representation of the helical bundle shown in panel B, where cylinders represent putative helices. Relative positions of residues 50, 83, and 173 are shown. (D) Three-dimensional representation of a hypothetical helical hairpin structure that is derived by a hinge-type opening around break in helix 2. This structure has the approximate dimensions that have been found experimentally through analytical ultracentrifugation and fluorescence measurements (*2*).

the context of the measurements obtained in the FRET experiments. That is, the mean FRET distances for the two amino acid pairs 50−83 and 50−173 are ∼21−22 Å. These distances are far smaller than the distances calculated from the hairpin model, 47−56 Å. On the other hand, the fact that the experimental FRET distances are somewhat longer than those measured on the helical bundle structure in Figure 9 may reflect the limitations of the model used or our inability to assign the side chain locations in the model. The

Table 6: C_α to C_α Distances, in Å, in Hypothetical Helical Bundle and Hairpin Structures[a]

residue pair	helical bundle	helical hairpin
W50−R83	10.0	46.8
W50−R173	15.5	56.5

[a] Distances were measured from 1AV1 PDB coordinates based on models shown in Figure 9.

purpose here is to present one possible model that may be critically evaluated as more structural information becomes available.

Clearly, there are many more ways to construct a bundle, and many of these hypothetical helix bundle structures would not be ruled out by two FRET measurements. The measurements reported here do not address nor are they inconsistent with (1) a close proximity or interaction between the N- and C-terminii (*13*, *15*, *16*, *19*, *41*, *42*) or (2) the presence of a two domain architecture (*9*, *12*, *14*, *18*, *21*), since the most C-terminal acceptor fluorophore is located at residue 173. However, a necessary constraint on any alternative model would be that a reversed turn exists some place between residues 50 and 83. Alternative models where this segment of the polypeptide is one continuous stretch of helix would exhibit a distance too great to match the 21−22 Å measured here. For example, the two FRET measurements we have obtained do not fit an alternative helical bundle model constructed by Sean Davidson and colleagues (*5*, *42*).

FRET Analysis of Molten Globules: What Can We Learn? A related question is, would an ensemble of globular helical structures, as envisaged to exist in a molten globule state, yield the same FRET *distance distributions* obtained here, thus rendering moot comparisons to a particular model? In other words, the single distribution fit supports a "single" conformation, the specific distances measured support the globular (helical bundle) conformation, and the narrow distance distribution supports the discrete (not molten) nature of the conformation. What range of distance distributions are found in the molten globule class? This question is difficult to address directly since there is not a body of the literature on molten globules to which we may compare our distance distributions. However, the following published accounts provide some insights.

Tcherkasskaya and Ptitsyn measured, by FRET, the distance between two tryptophans and two modified tyrosines, all within the AGH helix complex of apomyoglobulin in the molten globule state (*43*). Their earlier studies showed that this helix complex forms at an early stage of folding and exists in the molten globule state, and from their FRET studies, they found that the measured distances were within 1−2 Å of those observed in the X-ray crystal structure of native apomyoglobulin. No distance distributions were determined. This is an example of a molten globule ensemble of conformations that all share a common structural motif found in the native state (*37*). In a different approach, Lakshmikanth et al. used FRET methods to measure distance distributions between a single donor−acceptor pair (Trp 53 to a modified Cys 82) as a function of denaturant-induced unfolding of barstar (*44*). In these studies, nativelike intermediates, likened to a molten globule, were inferred by the progressive increase in the measured distance prior to complete unfolding. In the transition zone where the molten globule was thought to exist, distances measured were approximately 3 Å greater than found in the X-ray crystal structure and the half-widths of the distance distributions rose from ∼1 Å in the native state to ∼3−7 Å (depending on the denaturant) in the transition zone. A different perspective was obtained by Navon et al., who used FRET to measure distance distributions for 11 different donor−acceptor pairs within the early stages of RNase A folding, where an ensemble of partially folded compact conformers exist (*45*). For many of these conformers, the distance measured was 10 Å or more greater than observed in the X-ray crystal structure (absolute distances measured were 23−40 Å) and the half-widths of the distance distributions ranged from 18 to >40 Å. A majority of distances were significantly shorter than the estimated distance between the residues in a statistical coil state (some were shorter by 20 Å), indicating a significant degree of compactness.

From these studies, it may be concluded that distance distributions measured in a molten globule state can be remarkably narrow, or not, depending on the location of the residues and the nature of the folding intermediate. The practical conclusion for the present studies remains the same, which is the data are consistent with a discrete compact state.

Comparison of Present FRET Data with Previous FRET Data. The FRET data presented here may also be compared with FRET data obtained previously on lipid-free apo A-I (*16*, *17*). In those reports, energy transfer was measured to the extrinsic probe acrylodan from five tryptophans, four from the native apo A-I tryptophans at positions 8, 50, 72, and 108, and one from position −3 that arose from the inclusion of the apo A-I prosequence into the recombinant proteins. In these two reports, multiple constructs containing a single acrylodan at different locations were used to measure energy transfer from the constellation of five tryptophans within the protein. On the basis of the FRET distances, a hairpin structure was constructed that brings the carboxyl and amino terminus in close proximity. In those studies, donor lifetimes and energy transfers were necessarily an average from the five tryptophans. Therefore, the authors interpreted their results as a measure of the distance from the single acceptor site to a region of the protein in which the five tryptophans are located. Such a calculated distance based on the averaged lifetimes of the five donors is ill-defined because it is impossible to know how the individual tryptophans contribute to the average lifetimes and which ones participate in the energy transfer.

Conclusions. FRET measurements were taken from a single native tryptophan at position 50 to a single acceptor, AEDANS, at either position 83 or 173. These data have been interpreted in the context of two structural models for lipid-free apo A-I that were constructed using structural information on interhelical pairing obtained from the crystal structure of apo Δ(1−43)A-I. Of the two models, a globular helical bundle and an extended helical hairpin, the results are most consistent with the presence of single conformation in the form of a helical bundle. The validity of proposing a discrete bundle structure for apo A-I rather than an ensemble of globular structures comes from new DSC results that call into question the appropriateness of considering apo A-I a molten globule.

ACKNOWLEDGMENT

We thank Marion Kirk and the Comprehensive Cancer Center for mass spectroscopic analyses, and Jie Li for assistance with construction of the mutants. We also thank Drs. Danise Rogers and Linda Roberts for helpful discussions and Dr. Roberts for comments on the manuscript.

REFERENCES

1. Narayanaswami, V., and Ryan, R. O. (2000) Molecular basis of exchangeable apolipoprotein function. *Biochim. Biophys. Acta 1483*, 15−36.

2. Brouillette, C. G., Engler, J. A., Borhani, D. W., and Anantharamaiah, G. M. (2001) Structural models of human apolipoprotein A-I: a critical analysis and review. *Biochim. Biophys. Acta 1531*, 4−46.
3. Saito, H., Lund-Katz, S., and Phillips, M. C. (2004) Contributions of domain structure and lipid interaction to the functionality of exchangeable human apolipoproteins. *Prog. Lipid Res. 43*, 350−380.
4. Marcel, Y. L., and Kiss, R. S. (2003) Structure−function relationships of apolipoprotein A-I: a flexible protein with dynamic lipid associations. *Curr. Opin. Lipidol. 14*, 151−157.
5. Davidson, W. S., and Silva, G. D. (2005) Apolipoprotein structural organization in high-density lipoproteins: belts, bundles, hinges and hairpins. *Curr. Opin. Lipidol. 16*, 295−300.
6. Safi, W., Maiorano, J. N., and Davidson, W. S. (2001) A proteolytic method for distinguishing between lipid-free and lipid-bound apolipoprotein A-I. *J. Lipid Res. 42*, 864−872.
7. Rye, K.-A., and Barter, P. J. (2004) Formation and metabolism of prebeta-migrating, lipid-poor apolipoprotein A-I. *Arterioscler. Thromb. Vasc. Biol. 24*, 1−8.
8. Gursky, O., and Atkinson, D. (1996) Thermal unfolding of human high-density apolipoprotein A-1: implications for a lipid-free molten globular state. *Proc. Natl. Acad. Sci. U.S.A. 93*, 2991−2995.
9. Roberts, L. M., Ray, M. J., Shih, T.-W., Hayden, E., Reader, M. M., and Brouillette, C. G. (1997). Structural analysis of apolipoprotein A-I: limited proteolysis of methionine-reduced and -oxidized lipid-free and lipid-bound human apo A-I. *Biochemistry 36*, 7615−7624.
10. Borhani, D. W., Rogers, D. P., Engler, J. A., and Brouillette, C. G. (1997) Crystal structure of truncated human apolipoprotein A-I suggests a lipid-bound conformation. *Proc. Natl. Acad. Sci. U.S.A. 94*, 12291−96.
11. Rogers, D. P., Brouillette, C. G., Engler, J. A., Mishra, V. A., Anantharamaiah, G. M., Lund-Katz, S., Phillips, M. C., and Ray, M. J. (1997) Truncation of the amino terminus of human apolipoprotein A-I substantially alters only the lipid-free conformation. *Biochemistry 36*, 288−300.
12. Rogers, D. P., Roberts, L. M, Lebowicz, J., Engler, J. A., and Brouillette, C. G. (1998) Structural analysis of apolipoprotein A-I: effects of amino- and carboxy-terminal deletions on the lipid-free structure. *Biochemistry 37*, 945−55.
13. Rogers, D. P., Roberts, L. M., Lebowitz, J., Datta, G., Anantharamaiah, G. M., Engler, J. A., and Brouillette, C. G. (1998) The lipid-free structure of apolipoprotein A-I: effects of amino-terminal deletions. *Biochemistry 37*, 11714−25.
14. Davidson, W. S., Arngiv-McGuire, K., Kennedy, A., Josman, J., Hazlett, T. L., and Jonas, A. (1999) Structural organization of the N-terminal domain of apolipoprotein A-I: studies of tryptophan mutants. *Biochemistry 38*, 14387−14395.
15. Gorshkova, I. N., Liadaki, K., Gursky, O., Atkinson, D., and Zannis, V. I. (2000) Probing the lipid-free structure and stability of apolipoprotein A-I by mutation. *Biochemistry* 39, 15910−15919.
16. Tricerri, M. A., Agree, A. K. B., Sanchez, S. A., and Jonas, A. (2000) Characterization of apolipoprotein A-I structure using a cysteine-specific fluorescence probe. *Biochemistry 39*, 14682−14691.
17. Agree, A. K. B., Tricerri, M. A., McGuire, K. A., Tian, S.-M., and Jonas, A. (2002) Folding and stability of the C-terminal half of apolipoprotein A-I examined with a Cys-specific fluorescence probe. *Biochim. Biphys. Acta 1594*, 286−296.
18. Gorshkova, I. N., Liu, T., Zannie, V. I., and Atkinson, D. (2002) Lipid-free structure and stability of apolipoprotein A-I: probing the central region by mutation. *Biochemistry 41*, 10529−10539.
19. Fang, Y., Gursky, O., and Atkinson, D. (2003) Structural studies of N- and C-terminally truncated human apolipoprotein A-I. *Biochemistry 42*, 6881−6890.
20. Oda, M. N., Forte, T. M., Ryan, R. O., and Voss, J. C. (2003) The C-terminal domain of apolipoprotein A-I contains a lipid-sensitive conformational trigger. *Nat. Struct. Biol. 10*, 455−460.
21. Saito, H., Dhanasekaran, P., Nguyen, D., Holvoet, P., Lund-Katz, S., and Phillips, M. C. (2003) Domain structure and lipid interaction in human apolipoproteins A-I and E, a general model. *J. Biol. Chem. 278*, 23227−23232.
22. Chen, Y. H., Yang, J. T., and Martinez, H. M. (1972) Determination of the secondary structures of proteins by circular dichroism and optical rotatory dispersion. *Biochemistry 11*, 4120−4131.
23. Parker, C. A., and Rees, W. T. (1960) Correction of fluorescence spectra and measurement of fluorescence quantum efficiency. *Analyst (London) 85*, 587−600.
24. She, M., Dong, W.-J., Umeda, P. K., and Cheung, H. C. (1997) Time-resolved fluorescence study of the single tryptophans of engineered skeletal muscle troponin C. *Biophys. J. 73*, 1042−1055.
25. She, M., Xing, J., Dong, W.-J., Umeda, P. K., and Cheung, H. C. (1998) Calcium binding to the regulatory domain of skeletal muscle troponin C induces a highly constrained open conformation. *J. Mol. Biol. 281*, 445−452.
26. Lakowicz, J. R., Gryczynski, I., Cheung, H. C., Wang, C.-K., Johnson, M. L., and Josh, N. (1988) Distance distributions in proteins recovered by using frequency-domain fluorometry. Applications to troponin I and its complex with troponin C. *Biochemistry 27*, 9149−9160.
27. Cheung, H. C. In *Topics in Fluroescence Spectroscopy*, Lakowicz, J. R., Ed.; Plenum Press, New York, 1991; vol 2, pp 127−1776.
28. Cheung, H. C., Wang, C.-K., Gryczynski, I., Wiczk, W., Laczko, G., Johnson, M. L., and Lakowicz, J. R. (1991) Distance distributions and anisotropy decays of troponin C and its complex with troponin I. *Biochemistry 30*, 5238−5247.
29. Haas, E. E., Katchalsky-Katzir, E., and Steinberg, I. Z. (1978) Effect of the orientation of donor and acceptor on the probability of energy transfer involving electronic transitions of mixed polarization. *Biochemistry 17*, 5064−5070.
30. Torgerson, P. M., and Morales, M. F. (1984) Application of Dale-Eisenger analysis to proximity mapping in the contractile system. *Proc. Natl. Acad. Sci. U.S.A. 81*, 3723−3727.
31. Gursky, O. (2005) Apolipoprotein structure and dynamics *Curr. Opin. Lipidol. 16*, 287−294.
32. Arai, M., and Kuwajima, K. (2000) Role of the molten globule state in protein folding. *Adv. Prot. Chem. 53*, 209−282.
33. Pfeil, W., Bychkova, V. E., and Ptitsyn, O. B. (1986) Physical nature of the phase transition in globular proteins. Calorimetric study of human alpha-lactalbumin. *FEBS Lett. 198*, 287−291.
34. Griko, Y. V., and Privalov, P. L. (1994) Thermodynamic puzzle of apomyoglobin unfolding. *J. Mol. Biol. 235*, 1318−1325.
35. Carra, J. H., Anderson, E. A., and Privalov, P. L. (1994) Thermodynamics of staphylococcal nuclease denaturation. II. The A-state. *Prot. Sci. 3*, 952−959.
36. Quezada, C. M., Schulman, B. A., Froggatt, J. J., Dobson, C. M., and Redfield, C. (2004) Local and global cooperativity in the human alpha-lactalbumin molten globule. *J. Mol. Biol. 338*, 149−158.
37. Xie, D., and Freire, E. (1994) Molecular basis of cooperativity in protein folding. V. Thermodynamic and structural conditions for the stabilization of compact denatured states. *PROTEINS: Struc., Funct., Genet. 19*, 291−301.
38. Griko, Y. V., Freire, E., and Privalov, P. L. (1994) Energetics of the.alpha.-Lactalbumin States: A Calorimetric and Statistical Thermodynamic Study. *Biochemistry 33*, 1889−1899.
39. Ren, X., Zhao, L., Sivashanmugam, A., Miao, Y., Korando, L., Yang, Z., Reardon, C. A., Getz, G. S., Brouillette, C. G., Jerome, W. G., and Wang, J. (2005) Engineering mouse apolipoprotein A-I into a monomeric, active protein useful for structural determination, *Biochemistry 44*, 14907−14919.
40. Klon, A. E., Segrest, J. P., and Harvey, S. C. (2002) Comparative models for human apolipoprotein A-I bound to lipid in discoidal high-density lipoprotein particles. *Biochemistry 41*, 10895−10905.
41. Davidson, W. S., Hazlett, T., Mantulin, W. W., and Jonas, A. (1996) The role of apolipoprotein AI domains in lipid binding. *Proc. Natl. Acad. Sci. U.S.A. 93*, 13605−13610.
42. Silva, R. A. G. D., Hilliard, G. M., Fang, J., Macha, S., and Davidson, W. S. (2005) A three-dimensional molecular model of lipid-free apolipoprotein A-I determined by cross-linking/mass spectrometry and sequence threading. *Biochemistry 44*, 2759−69.
43. Tcherkasskaya, O., and Ptitsyn, O. B. (1999) Molten globule versus variety of intermediates: influence of anions on pH-denatured apomyoglobin. *FEBS Lett. 45*, 325−331.
44. Lakshmikanth, G. S., Sridevi, K., Krishnamoorthy, G., and Udgaonkar, J. B. (2001) Structure is lost incrementally during the unfolding of barstar. *Nat. Struct. Biol. 8*, 799−804.
45. Navon, A., Ittah, V., Landsman, P., Scheraga, H. A., and Haas, E. (2001) Distributions of Intramolecular Distances in the Reduced and Denatured States of Bovine Pancreatic Ribonuclease A. Folding Initiation Structures in the C−Terminal Portions of the Reduced Protein. *Biochemistry 40*, 105−118.

46. Segrest, J. P., Jones, M. K., DeLoof, H., Brouillette, C. G., Venkatachalapathi, Y. V., and Anantharamaiah, G. M. (1992) The amphipathic helix in the exchangeable apolipoproteins: a review of secondary structure and function. *J. Lipid Res. 33*, 141−166.
47. Okon, M., Frank, P. G., Marcel, Y. L., and Cushley, R. J. (2001) Secondary structure of human apolipoprotein A-I(1−186) in lipid-mimetic solution. *FEBS Lett 487*, 390−396.
48. Nolte, R. T., and Atkinson, D. (1992) *Biophys. J. 63*, 1221−1239.
49. Suurkuusk, M., and Hallén, D. (1999) Denaturation of apolipoprotein A-I and the monomer form of apolipoprotein A-I_{Milano}. *Eur. J. Biochem. 265*, 346−352.

BI051018V